Acta Pharmaceutica Sinica B 2022;12(7):3103−3112

Chinese Pharmaceutical Association
Institute of Materia Medica, Chinese Academy of Medical Sciences

Acta Pharmaceutica Sinica B

www.elsevier.com/locate/apsb
www.sciencedirect.com

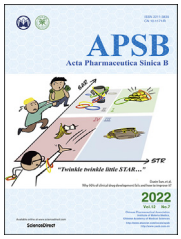

ORIGINAL ARTICLE

Structure-based discovery of orally efficient inhibitors *via* unique interactions with H-pocket of PDE8 for the treatment of vascular dementia

Xu-Nian Wu[a,†], Qian Zhou[a,†], Ya-Dan Huang[a], Xi Xie[b], Zhe Li[a], Yinuo Wu[a,*], Hai-Bin Luo[a,b,*]

[a]*School of Pharmaceutical Sciences, Sun Yat-sen University, Guangzhou, 510006, China*
[b]*Key Laboratory of Tropical Biological Resources of Ministry of Education and One Health Institute, School of Pharmaceutical Sciences, Hainan University, Haikou 570228, China*

Received 2 December 2021; received in revised form 20 January 2022; accepted 12 February 2022

KEY WORDS

Phosphodiesterase 8 (PDE8);
Vascular dementia;
Structure-based drug design;
MM-GB/SA;
Free energy prediction;
Structure−activity relationship;
Binding potencies

Abstract Our previous study demonstrated that phosphodiesterase 8 (PDE8) could work as a potential target for vascular dementia (VaD) using a chemical probe **3a**. However, compound **3a** is a chiral compound which was obtained by chiral resolution on HPLC, restricting its usage in clinic. Herein, a series of non-chiral 9-benzyl-2-chloro-adenine derivatives were discovered as novel PDE8 inhibitors. Lead **15** exhibited potent inhibitory activity against PDE8A (IC_{50} = 11 nmol/L), high selectivity over other PDEs, and remarkable drug-like properties (worthy to mention is that its bioavailability was up to 100%). Oral administration of **15** significantly improved the cAMP level of the right brain and exhibited dose-dependent effects on cognitive improvement in a VaD mouse model. Notably, the X-ray crystal structure of the PDE8A−**15** complex showed that the potent affinity and high selectivity of **15** might come from the distinctive interactions with H-pocket including T-shaped $\pi-\pi$ interactions with Phe785 as well as a unique H-bond network, which have never been observed in other PDE−inhibitor complex before, providing new strategies for the further rational design of novel selective inhibitors against PDE8.

© 2022 Chinese Pharmaceutical Association and Institute of Materia Medica, Chinese Academy of Medical Sciences. Production and hosting by Elsevier B.V. This is an open access article under the CC BY-NC-ND license (http://creativecommons.org/licenses/by-nc-nd/4.0/).

*Corresponding authors. Tel./fax: +86 20 39943062, +86 20 39943000
E-mail addresses: wyinuo3@mail.sysu.edu.cn (Yinuo Wu), hbluo@hainanu.edu.cn (Hai-Bin Luo).
†These authors made equal contributions to this work.
Peer review under responsibility of Chinese Pharmaceutical Association and Institute of Materia Medica, Chinese Academy of Medical Sciences

https://doi.org/10.1016/j.apsb.2022.02.012
2211-3835 © 2022 Chinese Pharmaceutical Association and Institute of Materia Medica, Chinese Academy of Medical Sciences. Production and hosting by Elsevier B.V. This is an open access article under the CC BY-NC-ND license (http://creativecommons.org/licenses/by-nc-nd/4.0/).

1. Introduction

Vascular dementia (VaD) has been regarded as the second most common type of dementia after Alzheimer's disease in the worldwide[1]. Cerebrovascular disease, ischemic or hemorrhagic brain injury will trigger the cognitive impairment in VaD patients[2,3]. Risk factors such as age, diabetes, and hypertension are also involved in the pathogenesis of VaD. Thus, the mechanism of VaD is complicated and still unclear. No specific medicine for VaD has been approved so far.

The cAMP/PKA and NO/cGMP/PKG signaling play a considerable role in the memory consolidation and long-term potentiation (LTP) of synaptic transmission[4−6]. The phosphodiesterases (PDEs), a superfamily in charge of hydrolyzing cAMP and cGMP, can be divided into eleven isoforms (PDE1−PDE11)[7]. The PDE4, PDE7, and PDE8 subtypes specially hydrolyze cAMP whereas the PDE5, PDE6, and PDE9 ones specially hydrolyze cGMP. The other subfamilies hydrolyze cAMP and cGMP, simultaneously. Many PDEs inhibitors could enhance the cognitive abilities in the mouse models of Alzheimer's disease, Parkinson's disease, schizophrenia, and etc., identifying PDEs as potential targets for memory improvement. For VaD, PDE3 inhibitor cilostazol could attenuated STZ diabetes induced VaD[8]. Recently, PDE4 inhibitor **4e** discovered by our group, showed the cognitive improvement abilities in the VaD mouse model[9].

Among all the PDEs, PDE8 showed the highest affinity for the hydrolysis of cAMP[10−13], indicating that PDE8 may be an efficient target for the cAMP-related diseases. However, only a few PDE8 inhibitors have been developed yet[14−16], and most of them are even non-selective, limiting the exploration of the biological functions of PDE8 and the recognition mechanism studies of inhibitors with PDE8. Most recently, our group developed a series of selective PDE8 inhibitors and identified that PDE8 could work as a potential drug target against VaD *via* a chemical probe **3a**[17]. However, **3a** was a chiral compound and was difficultly obtained by chiral resolution on HPLC.

With our continuous interest in the discovery of PDE8 inhibitors, structural optimization of compound **3a** was performed in this work (Fig. 1). A non-chiral compound **15** with potent affinity for PDE8 and high selectivity over other PDEs was obtained, which also showed remarkable drug-like properties and considerable memory improvement effects in the unilateral common carotid artery occlusion (UCCAO) mouse model. Notably, the cocrystal structure of **15** bound to PDE8 demonstrated that **15** formed distinctive interactions such as T-shaped $\pi-\pi$ interactions with Phe785 and a unique hydrogen bond network with PDE8, which might be the major reason for the potent inhibitory activity of **15** against PDE8 and high selectivity over other PDEs, providing evidence for the further development of PDE8 inhibitors.

2. Results and discussion

2.1. The process of design novel potent PDE8 inhibitors using X-ray structure

Compared with compound **3a** (PDE8A IC_{50}: 10 nmol/L), the non-chiral compound **2c** using the hydrogen atom instead of the (*S*)-methyl group of **3a**, only showed an IC_{50} value of 357 nmol/L against PDE8A[17]. Another non-chiral compound **10** (Table 1) showed an IC_{50} value of 117 nmol/L against PDE8A. In order to develop non-chiral PDE8 inhibitors with excellent inhibitory activities, compound **10** was selected as the hit compound, and the cocrystal of the PDE8A−**10** complex was obtained and analyzed for the rational design.

The binding pocket of PDE8 can divide into four subpockets like PDE4[18] and PDE2[19], including Q-pocket, M-pocket, S-pocket, and H-pocket (Fig. 2A). The 2-chloroadenine scaffold of **10** bound to Q-pocket, forming a $\pi-\pi$ stacking interaction with Phe781 as well as four hydrogen bonds with Gln778 and Asn729. Compared with **3a** forming a hydrogen bond with Tyr748, the difluoroethoxyl of **10** stretched deeper in H-pocket and formed a hydrogen bond with His673 instead of Tyr748 (Supporting Information Fig. S1). In addition, owing to the strong electron-withdrawing effects of two fluorine atoms, the adjacent C−H tended to perform positive electrostatic potential, and interacted with Asp726 and Thr668 through water-bridged hydrogen bonds. Furthermore, the benzyl of compound **10** formed T-shaped $\pi-\pi$ interactions with Phe781 and Phe785. To our knowledge, the hydrogen bond network and T-shaped $\pi-\pi$ interactions in H-pocket have never been observed in PDE-inhibitor complex before. We observed that compound **10** mainly occupied Q-pocket and H-pocket, but hardly interacted with S-pocket. Thus, substituents were introduced at the *meta*-position of benzyl group to occupy S-pocket (Fig. 2B), which might form extra interactions with the adjacent residues Phe785, Met764, Phe767, and Tyr748, enhancing the inhibitory activity of target compounds.

To accelerate the process of optimization, a MM-GB/SA approach was adopted to predict binding free energies ($\Delta G_{bind,pred}$) of designed compounds **11**−**25** with PDE8A (Table 1). Compared with hit **10** (−33.22 ± 3.46 kcal/mol), most designed

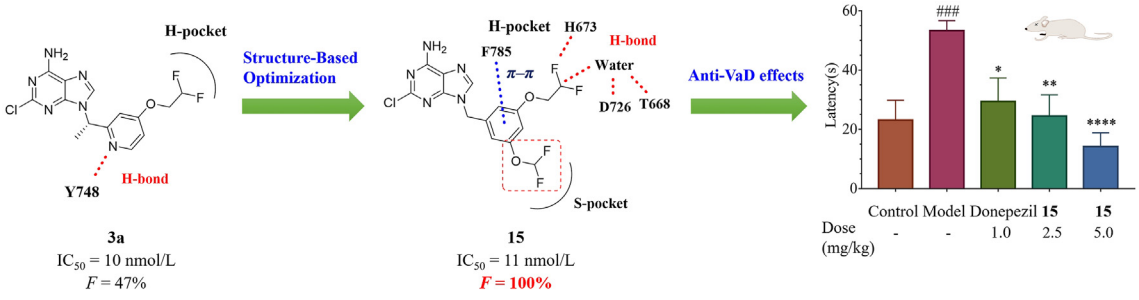

Figure 1 Structural optimization of non-chiral PDE8 inhibitors as anti-VaD agents.

Table 1 The prediction of binding free energies ($\Delta G_{bind,\ pred}$), IC_{50}, and metabolic stability RLM $t_{1/2}$ of target compounds.

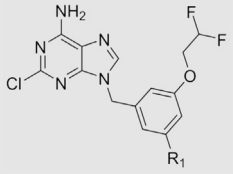

No.	R_1	$\Delta G_{bind,\ pred}$ (kcal/mol)	IC_{50} (nmol/L)[a]	RLM $t_{1/2}$ (min)
10	−H	−33.22 ± 3.46	117 ± 6	–
11	−F	−35.50 ± 2.31	51 ± 3	–
12	−OH	−32.14 ± 3.05	193 ± 17	–
13		−36.52 ± 2.85	591 ± 11	–
14		−37.27 ± 3.01	593 ± 69	–
15		−37.94 ± 2.85	11 ± 1	169
16		−40.93 ± 2.66	4.6 ± 0.6	6
17		−39.68 ± 2.66	5.0 ± 0.3	16
18		−43.03 ± 2.61	20 ± 2	–
19		−38.80 ± 2.42	40 ± 1	–
20		−41.17 ± 2.33	52 ± 5	–
21		−37.38 ± 3.02	597 ± 61	–
22		−43.04 ± 2.53	3.1 ± 0.2	8
23		−42.34 ± 3.27	4.8 ± 0.3	39
24		−41.24 ± 2.75	5.9 ± 0.6	27
25		−39.57 ± 2.78	13 ± 2	–

[a]Data are given as mean ± SD ($n \geq 3$).

compounds showed more negative $\Delta G_{bind,\ pred}$ values, except for compound **12** (−32.14 ± 3.05 kcal/mol) with a comparable $\Delta G_{bind,\ pred}$ value.

A PAINS-Remover[20] (https://www.cbligand.org/PAINS/) screening was performed to avoid the pan assay interference compounds (PAINS), and all compounds satisfied the filter test and were synthesized.

2.2. *Structure–activity relationships (SARs) of target compounds*

Compared with the initial hit **10** (IC_{50} = 117 nmol/L), compound **11** with F atom at the R_1 position exhibited a slightly better IC_{50} value of 51 nmol/L while compound **12** with a hydroxyl group showed a comparable IC_{50} value of 193 nmol/L against PDE8A.

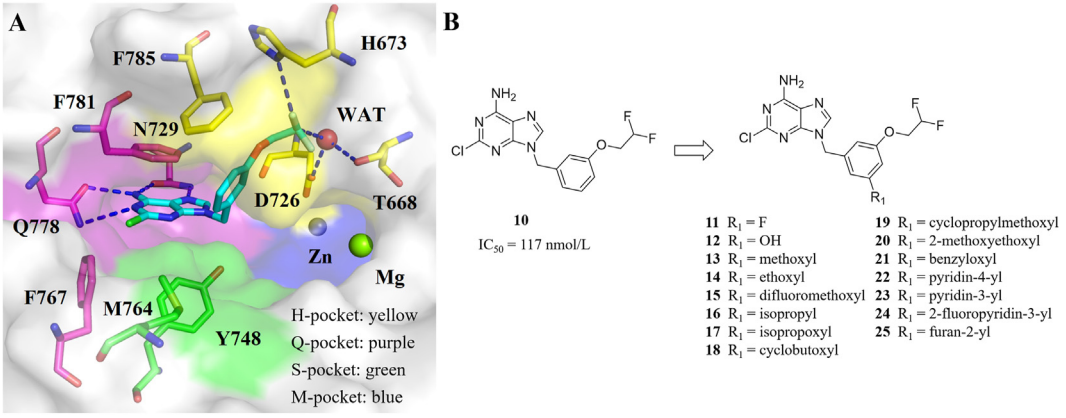

Figure 2 (A) Surrounding residues of four subpockets represents by four different colors in the PDE8A–**10** complex (PDB ID: 7VSL). (B) Rational design of potent PDE8 inhibitors.

Table 2 Selectivity index of **15** against PDE subtypes.

PDE subtype	**15**		**3a**	
	IC_{50} (nmol/L)[a]	Selectivity index	IC_{50} (nmol/L)[b]	Selectivity index
PDE8A1 (480−820)	11 ± 1	/	10 ± 1	/
PDE1C (147−531)	6179 ± 429	562	3095 ± 495	310
PDE2A (580−919)	4315 ± 171	392	2177 ± 104	218
PDE3A (679−1087)	>10,000	>909	>10,000	>1000
PDE4D2 (86−413)	5485 ± 486	499	7148 ± 340	715
PDE5A1 (535−860)	4835 ± 353	440	>10,000	>1000
PDE7A1 (130−482)	4853 ± 359	441	>10,000	>1000
PDE9A2 (181−506)	>10,000	>909	>10,000	>1000
PDE10A (449−770)	1224 ± 28	111	4436 ± 160	444

[a]Data are given as mean ± SD ($n \geq 3$).
[b]Data reported from our previous report[17]. except the data of PDE1C, which was determined in this research.

Both compound **13** with a methoxyl group and **14** with an ethoxyl group showed similar inhibitory activities against PDE8A. Compared with **13**, **15** with a difluoromethoxyl group demonstrated significant increasement of the inhibitory potency, indicating that fluorine atom is in favor of S-pocket.

After changing the methoxyl group of **13** to substituents with larger volume of isopropyl (**16**) and isopropoxyl (**17**), the inhibitory activities against PDE8A were significantly improved. However, further increasing the volume of R_1 substituents, such as cyclobutoxyl (**18**), cyclopropylmethoxyl (**19**), 2-methoxyethoxyl (**20**) and benzyloxyl (**21**), resulted in decreased inhibitory activities against PDE8A. Thus, the steric effect of R_1 substituents played an important role when binding S-pocket. Isopropyl and isopropoxyl groups, with appropriate volume, were preferred for binding with S-pocket.

In order to enhance the $\pi-\pi$ interactions with Phe781 and Phe785, compounds **22**−**25** with aromatic heterocycles at the R_1 position were designed. As expected, all these compounds showed significantly increased inhibitory activities against PDE8A compared with compound **10**. Compounds **22** with 4-pyridinyl, **23** with 3-pyridinyl, and **24** with 2-fluoropyridin-3-yl groups gave the IC_{50} values of 3.1, 4.8, and 5.9 nmol/L against PDE8A,

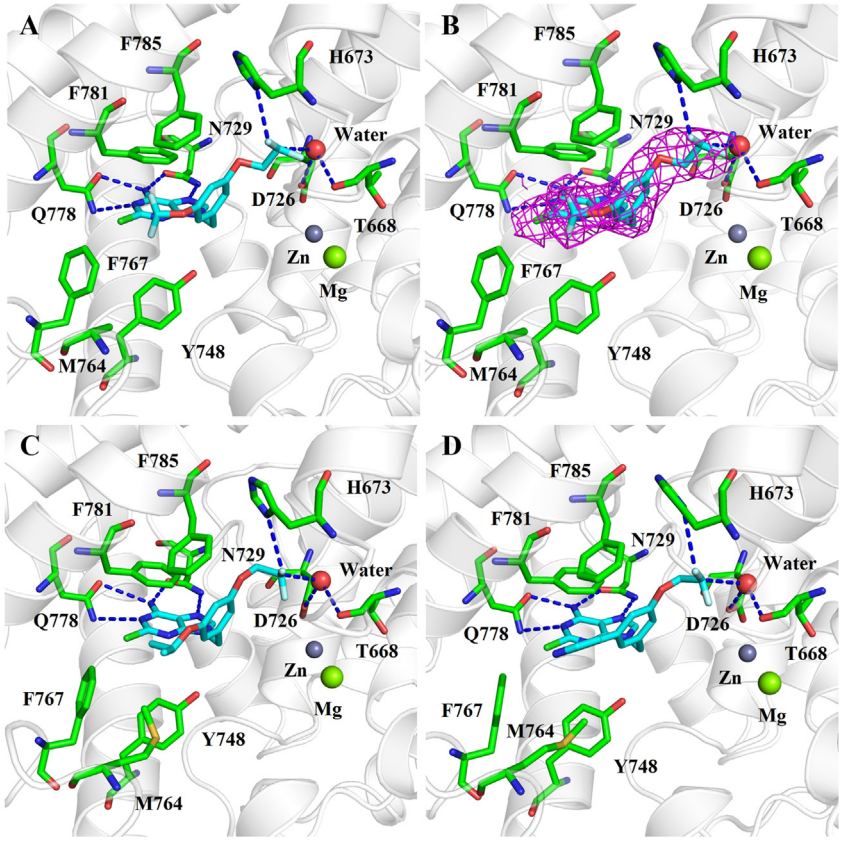

Figure 3 The cocrystal structures of **15**, **17**, and **22** with PDE8A. (A) The binding pattern of PDE8A-**15** complex (PDB ID: 7VTV). **15** is shown as cyan sticks and the key residues are shown as green sticks. (B) Omit *Fo*−*Fc* electron density map of **15** at a contour level of 1.0σ. (C) The binding pattern of PDE8A−**17** complex (PDB ID: 7VTW). (D) The binding pattern of PDE8A−**22** complex (PDB ID: 7VTX).

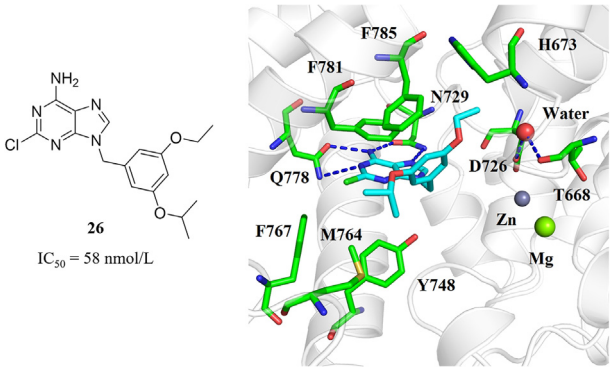

Figure 4 Compound **26** and its predicted binding mode with PDE8.

respectively. Compound **25** with a smaller π-conjugated 2-furyl core afforded a relatively low inhibitory activity with an IC_{50} value of 13 nmol/L against PDE8A.

The predicted binding free energies ($\Delta G_{bind,\ pred}$) of target compounds were outlined in Table 1. The experimental binding free energies ($\Delta G_{bind,\ exp}$) were calculated by the IC_{50} values against PDE8A ($\Delta G_{bind,\ exp} \approx RT\ lnIC_{50}$). A linear correlation achieved (Supporting Information Fig. S2) a considerable Pearson correlation coefficient ($r = 0.68$) between $\Delta G_{bind,\ pred}$ and $\Delta G_{bind,\ exp}$, which demonstrated the MM-GB/SA approach could be efficiently applied to predict the $\Delta G_{bind,\ pred}$ and thus could save the synthesis plus bioassay efforts.

2.3. *The evaluation of metabolic stability by the rat liver microsomes (RLM)*

The metabolic stability of most potent compounds including **15**, **16**, **17**, **22**, **23**, and **24** were evaluated by the rat liver microsomes (RLM). Compound **16** with an isopropyl group and compound **17** with an isopropoxyl group gave the $t_{1/2}$ values of 6 min and 16 min, respectively, revealing that aromatic hydrocarbon and alkyl aryl ether are unstable in the present of RLM. Due to the fluorine atom's blocking effect in metabolic oxidation, compound **15** (R_1 = difluoromethoxyl) showed a great metabolic stability ($t_{1/2}$ = 169 min). Compounds **22**, **23**, and **24** gave the $t_{1/2}$ values of 8, 39, and 27 min, respectively, indicating that 3-pyridinyl derivatives are more stable than 4-pyridinyl derivatives. Thus compound **15** was subsequently subjected to other evaluations.

2.4. *Remarkable selectivity index of compound **15***

The selectivity profile of compound **15** over other PDEs was evaluated and the results are outlined in Table 2. Similar to **3a**, compound **15** also exhibited remarkable selectivity index. The selectivities against PDE3A and PDE9A2 were more than 900-fold. Its values of selectivity index against PDE1C, PDE2A, PDE4D2, PDE5A1, PDE7A1, and PDE10A were 562-, 392-, 500-, 437-, 441-, and 111-fold, respectively. These results demonstrated that compound **15** exhibits high selectivity over other PDEs, thus is suitable for the further development as a lead compound.

Table 3 Pharmacokinetic profiles of **15** in SD rats.

Parameters	*p.o.* (5.0 mg/kg)	i.v. (2.5 mg/kg)
$t_{1/2}$ (h)	7.92 ± 0.50	5.37 ± 0.86
T_{max} (h)	6.67 ± 2.31	
C_{max} (ng/mL)	1560 ± 223	
$AUC_{(0-t)}$ (h·ng/mL)	20,544 ± 2779	10,142 ± 635
$AUC_{(0-\infty)}$ (h·ng/mL)	23,665 ± 2970	10,611 ± 852
$MRT_{(0-t)}$ (h)	13.4 ± 0.4	7.81 ± 1.18
F (%)	100	

Table 4 Drug-like profiles of **15**.

Parameter	Value
*c*log*P*[a]	3.4
tPSA[a]	84
Solubility (pH 7.3)[b]	4 μg/mL
Human plasma protein binding	97.6%
Unbound brain concentration[c]	114 ng/g
Cytochrome P450 inhibition (IC_{50})	
CYP2C19	19 μmol/L
CYP2C9, 2D6, 1A2	>25 μmol/L
CYP3A4-M, 3A4-T	>50 μmol/L
*h*ERG inhibition (IC_{50})	>40 μmol/L
Acute toxicity	>1.5 g/kg

[a]*c*Log*P* and tPSA were predicted by Discovery Studio.
[b]The solubility was tested by HPLC.
[c]After an oral dose of 5.0 mg/kg at 4 h in C57BL/6J mice.

2.5. *Unique interactions observed in the cocrystal structure of **15** bound to PDE8*

The crystal structures of complexes of PDE8−**15**, PDE8−**17**, and PDE8−**22** (Fig. 3) were obtained, respectively. These three compounds adopted similar binding modes with PDE8 to hit **10**.

The 2-chloroadenine core of compound **15** occupied Q-pocket and formed $\pi-\pi$ interactions, van der Waals interactions, and H-bond interactions with Q-pocket. Its benzyl motif occupied H-pocket. Furthermore, it maintained the T-shaped $\pi-\pi$ interaction with Phe785 and H-bond network (a direct H-bond with His673 and water-bridged hydrogen bonds with Asp726 and Thr668) in H-pocket. As mentioned above, these interactions have never been observed in PDE−inhibitor complex before. The difference between lead **15** and hit **10** is that the difluoromethoxyl group of **15** occupied S-pocket as our designed. Some part of compound **15** even stretched toward the edge of Q-pocket, forming van der Waals interactions plus hydrophobic interactions with Phe781, Phe785, Phe767, Tyr748, and Met764 (the side chain of Met764 is missing when analyzing the crystal structure).

In order to validate the importance of unique H-bond network, we modified the difluoroethoxyl group of **17** (IC_{50} = 5.0 nmol/L) to an ethoxyl group of **26** (Fig. 4). The IC_{50} value of **26** dropped to 58 nmol/L, indicating that the H-bond network is in favor of ligand binding. In addition, we found that Phe785 in PDE8 is a unique residue according to the comparison of residues in H-pocket by sequence alignment (Supporting Information Table S1). Only PDE8 includes the residue with aromatic side chain (phenylalanine) at position 785, while other PDEs with alkyl side chains. The unique $\pi-\pi$ interaction with Phe785 and H-bond network may account for the high selectivity of **15**, providing a novel approach for the discovery of potent PDE8 inhibitors with high selectivity index.

2.6. *Remarkable drug-like profiles of **15***

In terms of the inhibitory activity, selectivity index, and metabolic stability, compound **15** was further subjected to evaluate

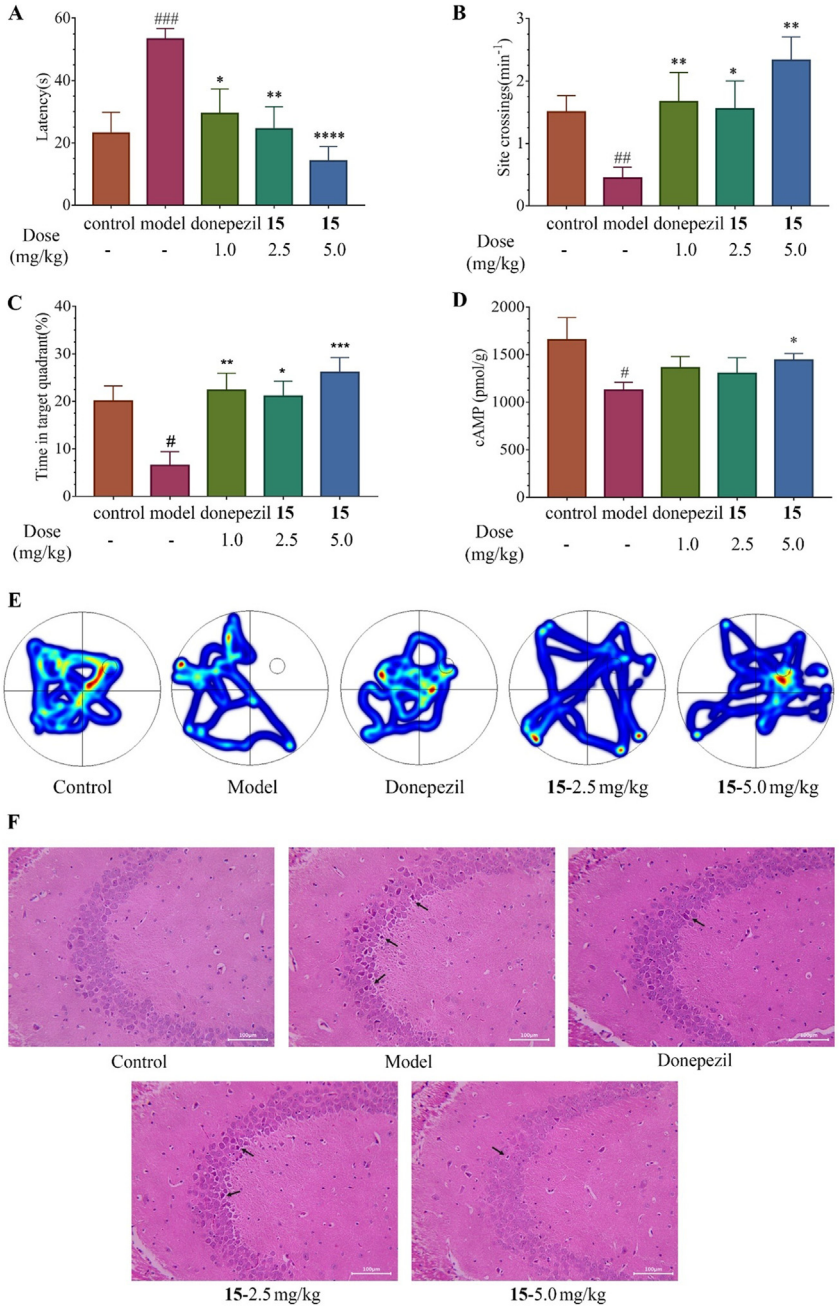

Figure 5 The cognitive impairment of UCCAO mice has been improved after orally administration with compound **15** at the doses of 2.5 mg/kg and 5.0 mg/kg. (A) Escape latency time of mice (s). (B) Site crossings (min^{-1}). (C) Time in the target quadrant (%). (D) cAMP levels of the right brain in mouse (pmol/g). (E) Image is representative trajectories from each group. (F) Representative images of each group with hematoxylin and eosin straining in hippocampal CA3 region (HE, × 200). Donepezil at a dose of 1.0 mg/kg was probed as a positive control. Scale bar: 100 μm. Data are represented as mean values ± SEM (n = 8−12 in each group). $^{\#}P < 0.05$ *vs* control; $^{\#\#}P < 0.01$ *vs* control; $^{\#\#\#}P < 0.001$ *vs* control; $^{*}P < 0.05$ *vs* model; $^{**}P < 0.01$ *vs* model; $^{***}P < 0.001$ *vs* model; $^{****}P < 0.0001$ *vs* model, respectively.

pharmacokinetic (PK) profile using SD rats (Table 3). After an oral dose of 5.0 mg/kg, **15** exhibited a moderate half-life of 7.92 h and an excellent bioavailability (F) of 100%. The C_{max} and $AUC_{(0-\infty)}$ of compound **15** were 1560 ng/mL and 23,665 h ng/mL, indicating that **15** had a high level of exposure *in vivo*. The plasma concentration of compound **15** was still up to 275 ng/mL at 24 h after the oral administration, which was 62 times of its IC_{50} value.

We further examined other drug-like profiles of **15**, including solubility, human plasma protein binding (PPB), unbound brain concentration, cytochrome P450 (CYP450) inhibition, *h*ERG inhibition, and acute toxicity (Table 4). The human PPB of **15** was 97.6%. The inhibition against CYP450 and *h*ERG were weak, and no acute toxicity was observed for an oral dose of 1.5 g/kg. After an oral dose of 5.0 mg/kg at 4 h in C57BL/6J mice, the brain concentration of **15** in the brain homogenates was 114 ng/g (about 281 nmol/L), which is

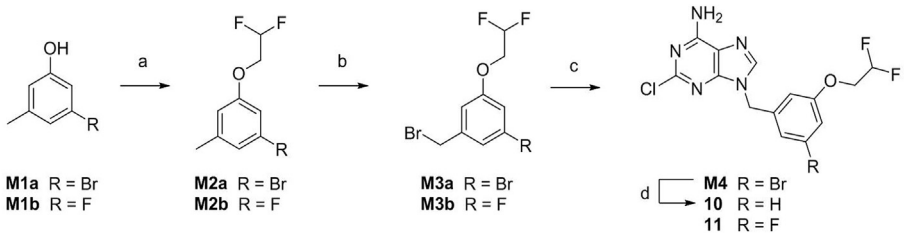

Scheme 1 Synthetic route for compounds **10** and **11**. Reagents and conditions: (a) 2-bromo-1,1-difluoroethane, cesium carbonate, acetonitrile, reflux, overnight; (b) *N*-bromosuccinimide, azodiisobutyronitrile, carbon tetrachloride, reflux, 4 h; (c) 2-chloro-9*H*-purin-6-amine, cesium carbonate, *N*,*N*-dimethylformamide, 70 °C, overnight; (d) Pd/C, H_2, methanol/tetrahydrofuran, r.t., overnight.

much higher than the IC_{50} (11 nmol/L) of **15** and strong enough to active the cAMP signal for memory improvement.

Compared with the PDE8 inhibitors **24** (IC_{50} = 43 nmol/L) reported by Pfizer[15,16], lead **15** achieved the excellent and higher inhibitory activity (IC_{50} = 11 nmol/L) against PDE8A and high selectivity over other PDEs. In addition, the pharmacokinetic profiles such as oral bioavailability and metabolic stability have been also improved. Furthermore, lead **15** had considerable brain penetrability and physicochemical properties (tPSA: 84, *c*log*P*: 3.4), which is more suitable to be developed for the CNS diseases.

2.7. *Significant therapeutic effects in VaD mice*

It is well demonstrated that mice treated with permanent UCCAO would lead to chronic hypoperfusion and ischemic injury including ischemic white matter (WM) lesions and lacunes[21,22]. Thus, a VaD mouse model with the right common carotid artery occlusion was adopted. After treatment with vehicle, compound **15** (2.5 and 5.0 mg/kg, *p.o.*) and donepezil (1.0 mg/kg, *p.o.*) for 3 weeks, respectively, the learning and memory ability was evaluated by Morris water maze (MWM) test. After removing the platform on the spatial probe trial day, the trajectories of each mouse were recorded, and the escape latency time (ELT) to find the platform site of each mouse, the number of the platform site crossings, and residence time in the target quadrant were analyzed.

As shown in Fig. 5, the ELT of the model group significantly increased in comparison with the control group. Meanwhile, the number of the platform site crossings was notably decreased compared with the control group and the identical trend was

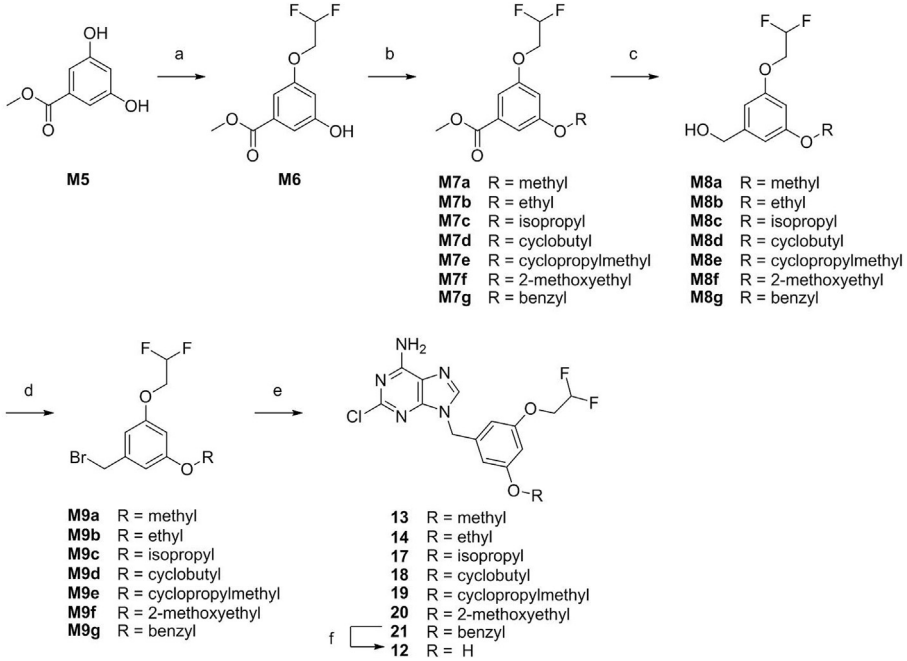

Scheme 2 Synthetic route for compounds **12**−**14** and **17**−**21**. Reagents and conditions: (a) 2-bromo-1,1-difluoroethane, potassium iodide, potassium carbonate, acetonitrile, reflux, overnight; (b) alkyl bromides or benzyl bromide, cesium carbonate, acetonitrile, reflux, overnight; (c) lithium aluminum hydride, tetrahydrofuran, r.t., 4 h; (d) phosphorus tribromide, dichloromethane, 0 °C to r.t., 4 h; (e) 2-chloro-9*H*-purin-6-amine, cesium carbonate, *N*,*N*-dimethylformamide, 70 °C, overnight; (f) Pd/C, H_2, methanol/tetrahydrofuran, r.t., overnight.

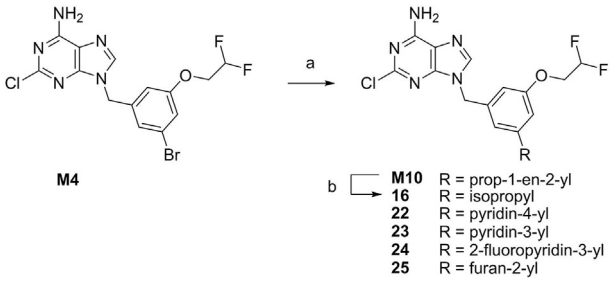

Scheme 3 Synthetic route for compounds **16** and **22**−**25**. Reagents and conditions: (a) aromatic boric acids or pinacol vinylboronate, [1,1′-bis(diphenylphosphino)ferrocene]dichloropalladium(II), potassium carbonate, 1,4-dioxane/water, 100 °C, overnight; (b) Pd/C, H_2, methanol/tetrahydrofuran, r.t., overnight.

observed in residence time in the target quadrant, which strongly demonstrated that the cognitive impairment occurred in UCCAO-treated mice and the VaD mouse model was built successfully.

Compared with the model group, oral administration with compound **15** at the dose of 2.5 and 5.0 mg/kg as well as the positive control donepezil at the dose of 1.0 mg/kg markedly decreased the ELT after the platform was removed in the spatial probe trial day. Furthermore, a significant increase was observed in the number of the platform site crossings in **15**-treated and donepezil-treated mice and the similar trend came to the residence time in the target quadrant. These results indicated that learning and memory functions had been improved in those mice. Besides, oral administration of **15** at 5.0 mg/kg daily showed a better ELT than that of 2.5 mg/kg. Consistently, the same dose responses in their therapeutic effects were observed on the number of the platform site crossings and residence time in the target quadrant. We also measured the concentration of cAMP in the right brain of all groups (Fig. 5D). Brain tissue cAMP levels of the model group were significantly decreased in comparison with the control group. Meanwhile, both low and high dose of **15** treatments upregulated the level of cAMP.

The histological changes were observed using the HE staining method. Compared with the control group with hippocampus neurons tightly arranged in a rounded shape and clear nucleolus, the neurons in model groups were shrunken or lost with scattered arrangement. The treatment of **15** clearly reduced the shrunken or

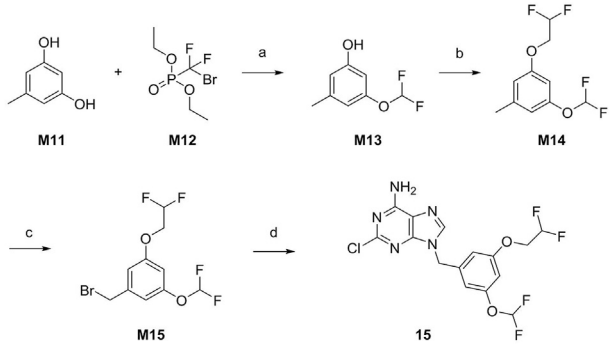

Scheme 4 Synthetic route for compound **15**. Reagents and conditions: (a) potassium hydroxide, acetonitrile/water, 1 h; (b) 2-bromo-1,1-difluoroethane, cesium carbonate, acetonitrile, reflux, overnight; (c) *N*-bromosuccinimide, azodiisobutyronitrile, carbon tetrachloride, reflux, 4 h; (d) 2-chloro-9*H*-purin-6-amine, cesium carbonate, *N*,*N*-dimethylformamide, 70 °C, overnight.

irregular neurons and decreased the neurons loss as the positive control donepezil. All these results suggested that lead **15** showed notable therapeutic effects on cognitive impairment improvement and efficiently improved the spatial learning and memory ability in VaD mouse model, which identified lead **15** as a novel PDE8 inhibitor for VaD treatment.

2.8. *Chemistry*

The synthetic routes for target compounds are depicted in Schemes 1−4. The key intermediate **M4** was synthesized by a process starting from the substitution of 3-bromo-5-methylphenol (**M1a**) with 2-bromo-1,1-difluoroethane, followed by Wohl−Ziegler bromination[23,24] and then coupling to 2-chloro-9*H*-purin-6-amine using cesium carbonate. Intermediate **M4** was treated with Pd-C/H_2 to give **10**. The synthesis of compound **11** was similar to that of **M4** using 3-fluoro-5-methylphenol as starting material (Scheme 1).

For the preparation of compounds **12**−**14** and **17**−**21** (Scheme 2), methyl 3,5-dihydroxybenzoate (**M5**) was substituted by 2-bromo-1,1-difluoroethane, followed by substitution with corresponding alkyl bromides or benzyl bromide to give **M7a**−**g**. The esters **M7a**−**g** were reduced using lithium aluminum hydride to yield alcohols **M8a**−**g**. The alcohols **M8a**−**g** were brominated using phosphorus tribromide to give benzyl bromide derivatives **M9a**−**g**, followed by coupling to 2-chloro-9*H*-purin-6-amine using cesium carbonate to produce target compounds **13**−**14** and **17**−**21**. Reduction of compound **21** with H_2 and Pd/C as a catalyst gave compound **12**.

As shown in Scheme 3, compounds **M10** and **22**−**25** were synthesized by Suzuki coupling[25] of intermediate **M4** with aromatic boric acids or pinacol vinylboronate in the presence of potassium carbonate as a base and Pd(dppf)$Cl_2 \cdot CH_2Cl_2$ as a catalyst. Then, reaction of **M10** with H_2 and Pd/C produced compound **16**.

The synthesis of compound **15** is shown in Scheme 4. The starting material 5-methylbenzene-1,3-diol (**M11**) was subjected to difluoromethylation, difluoroethylation, bromination and coupling to 2-chloro-9*H*-purin-6-amine to obtain compound **15**.

3. Conclusions

Herein, we performed structure-based optimization on compound **3a**, affording a series of non-chiral PDE8 inhibitors. Lead **15** showed potent inhibitory activity against PDE8A (IC_{50} = 11 nmol/L) and high selectivity profile against other PDE isoforms. The cocrystal structure of PDE8-**15** revealed a novel binding pattern including a T-shaped $\pi-\pi$ interaction with Phe785 and hydrogen bond network with H-pocket, providing new evidences to design highly selective PDE8 inhibitors. In addition, lead **15** exhibited remarkable drug-like properties like a bioavailability of 100% and its oral administration improved the cAMP level of the right brain, and exhibited dose-dependent effects on the improvement of spatial learning and memory capability in VaD mouse model.

4. Experimental

4.1. *Chemistry*

The synthetic routes and characterization data of target compounds were provided in Supporting Information.

4.2. Molecular modeling

The cocrystal structure of the PDE8−**10** complex (PDB ID: 7VSL) was chosen for molecular modeling. All target compounds were directly constructed on the basis of the conformation of **10** bound to PDE8. The procedures for molecular dynamics (MD) simulation were same as our previous studies[26,27]. For each protein-ligand system, 8 ns MD simulations were carried out by NPT ensemble with pressure of 1 atm and temperature of 300 K under periodic boundary conditions. The bonds with hydrogen atoms were restrained by SHAKE algorithm so that the time step was set to two fs[28,29]. The long-range electrostatic interactions was treated by the partial mesh Ewald (PME) method with a cutoff of 8 Å[30,31]. After 8 ns MD simulation, the binding free energy was predicted by the MM-GB/SA approach[32−34] in Amber 20[35] suite using 100 snapshots from 7 to 8 ns trajectory.

4.3. Protein expression and purification

The PDE8A protein was expressed and purified by the previously reported protocols[17]. *E. coli* BL21 (Codonplus, DE3) cells harboring the recombinant pET15b-*PDE8A1* plasmid (480−820)[36,37] were cultured in 2 × YT medium at 37 °C until OD_{600} = 0.6−0.8, followed by induction with isopropyl-*β*-D-thiogalactopyranoside (IPTG, 0.1 mmol/L) at 25 °C for one day. The pellet was denatured in guanidine (7.8 mmol/L) and Tris-HCl (0.1 mmol/L, pH 8.0) for 12 h, and then purified by the nickel nitriloacetic acid (Ni-NTA) column (Qiagen). The elution was added dropwise into the refolding buffer and carried out without swinging at 4 °C for 72 h, followed by purification using hydroxyapatite HTP GEL (Bio-Rad), Q-Sepharose column (GE Healthcare) and a gel filtration column Sephacryl S_{100} (GE Healthcare).

Other PDE isoforms were expressed and purified by similar procedures without denaturing and refolding process as our previous papers[9,17,27,38−41].

4.4. Bioassay test and crystallization

^{3}H-cAMP, the substrate for PDE8A, was diluted with the buffer containing Tris-HCl (20 mmol/L, pH 7.5), manganese chloride (10 mmol/L), and dithiothreitol (1 mmol/L) to about 20,000 cpm per assay. The mixture was reacted at 25 °C for 15 min and then terminated by adding zinc sulphate, following by barium hydroxide. The radioactivity of unreacted ^{3}H-cAMP in the supernatant was tested by a PerkinElmer 2910 liquid scintillation counter. The IC_{50} was fitted by nonlinear regression using at least eight different concentrations. Each test was measured at least three times.

Same procedures for crystallization were performed as previous report[9,17,38−40]. And the details of diffraction data and structure refinement statistic were given in Supporting Information Table S2.

4.5. Drug-like profiles determinations

The procedures for the determination of RLM stability, PK properties, human PPB, CYP450 inhibition, *h*ERG inhibition, and acute toxicity were same as our previous studies[17,38−40].

4.6. UCCAO mouse model and Morris water maze test

The similar experiments (Supporting Information) have been performed as our previously reported protocols[9,17]. All animal care and experimental protocols were in accordance with the "Guide for the Care and Use of Laboratory Animals" (National Institutes of Health Publication, revised 1996, No. 86-23, Bethesda, MD) and approved by the Institutional Ethical Committee for Animal Research of Sun Yat-sen University (IACUC number: SYSU-IACUC-2021-000129).

4.7. cAMP concentration assay

The mice' brains were quickly removed, immediately frozen in liquid nitrogen and then stored at −80 °C before tested. The competitive enzyme immunoassay was used to measure the cAMP levels (ADI-900-163, Enzo Life Sciences, Exeter, UK). Brain tissue homogenized in 0.1 mol/L HCl with 10 volumes. After centrifuge for 10 min, the supernatant was diluted to 5 times with 0.1 mol/L HCl and then tested by non-acetylated protocol.

Acknowledgments

This work was supported by the Natural Science Foundation of China (21877134, 22077143, 81903542,and 21977127), Science Foundation of Guangzhou City (201904020023, China), Fundamental Research Funds for Hainan University (KYQD(ZR)-21031, China), Science Foundation of Guangdong Province (2019A1515011883, China), Local Innovative and Research Teams Project of Guangdong Pearl River Talents Program (2017BT01Y093, China),and Guangdong Province Higher Vocational Colleges & Schools Pearl River Scholar Funded Scheme (2016, China). We cordially thank Prof. Hengming Ke from Department of Biochemistry and Biophysics at University of North Carolina, Chapel Hill, for his assistance with the molecular cloning, expression, purification, determination of the crystal structures, and bioassay of PDEs.

Author contributions

Xu-Nian Wu and Qian Zhou contributed equally to this work, lead the research, data analysis, and writing of the manuscript. Ya-Dan Huang and Xi Xie performed the biological tests. Zhe Li performed molecular docking and dynamic simulation calculations. Yinuo Wu and Hai-Bin Luo supervised the entire research with conceptualization, analysis and resources.

Conflicts of interest

The authors declare no competing financial interest.

Appendix A. Supporting information

Supporting data to this article can be found online at https://doi.org/10.1016/j.apsb.2022.02.012.

References

1. O'Brien JT, Thomas A. Vascular dementia. *Lancet* 2015;**386**:1698−706.

2. Kalaria RN. Neuropathological diagnosis of vascular cognitive impairment and vascular dementia with implications for Alzheimer's disease. *Acta Neuropathol* 2016;**131**:659−85.
3. Wardlaw JM, Smith C, Dichgans M. Mechanisms of sporadic cerebral small vessel disease: insights from neuroimaging. *Lancet Neurol* 2013; **12**:483−97.
4. Abel T, Nguyen PV, Barad M, Deuel TA, Kandel ER, Bourtchouladze R. Genetic demonstration of a role for PKA in the late phase of LTP and in hippocampus-based long-term memory. *Cell* 1997;**88**:615−26.
5. Vitolo OV, Sant'Angelo A, Costanzo V, Battaglia F, Arancio O, Shelanski M. Amyloid beta-peptide inhibition of the PKA/CREB pathway and long-term potentiation: reversibility by drugs that enhance cAMP signaling. *Proc Natl Acad Sci U S A* 2002;**99**:13217−21.
6. Ryan MM, Ryan B, Kyrke-Smith M, Logan B, Tate WP, Abraham WC. Temporal profiling of gene networks associated with the late phase of long-term potentiation *in vivo*. *PLoS One* 2012;**7**:e40538.
7. Beavo JA. Cyclic nucleotide phosphodiesterases: functional implications of multiple isoforms. *Physiol Rev* 1995;**75**:725−48.
8. Kumar A, Kumar A, Jaggi AS, Singh N. Efficacy of cilostazol a selective phosphodiesterase-3 inhibitor in rat model of streptozotocin diabetes induced vascular dementia. *Pharmacol Biochem Behav* 2015; **135**:20−30.
9. Liang J, Huang YY, Zhou Q, Gao Y, Li Z, Wu D, et al. Discovery and optimization of α-mangostin derivatives as novel PDE4 inhibitors for the treatment of vascular dementia. *J Med Chem* 2020;**63**:3370−80.
10. Lakics V, Karran EH, Boess FG. Quantitative comparison of phosphodiesterase mRNA distribution in human brain and peripheral tissues. *Neuropharmacology* 2010;**59**:367−74.
11. Soderling SH, Bayuga SJ, Beavo JA. Cloning and characterization of a cAMP-specific cyclic nucleotide phosphodiesterase. *Proc Natl Acad Sci U S A* 1998;**95**:8991−6.
12. Gamanuma M, Yuasa K, Sasaki T, Sakurai N, Kotera J, Omori K. Comparison of enzymatic characterization and gene organization of cyclic nucleotide phosphodiesterase 8 family in humans. *Cell Signal* 2003;**15**:565−74.
13. Fisher DA, Smith JF, Pillar JS, St Denis SH, Cheng JB. Isolation and characterization of PDE8A, a novel human cAMP-specific phosphodiesterase. *Biochem Biophys Res Commun* 1998;**246**:570−7.
14. Demirbas D, Wyman AR, Shimizu-Albergine M, Cakici O, Beavo JA, Hoffman CS. A yeast-based chemical screen identifies a PDE inhibitor that elevates steroidogenesis in mouse leydig cells *via* PDE8 and PDE4 inhibition. *PLoS One* 2013;**8**:e71279.
15. DeNinno MP, Wright SW, Visser MS, Etienne JB, Moore DE, Olson TV, et al. 1,5-Substituted nipecotic amides: selective PDE8 inhibitors displaying diastereomer-dependent microsomal stability. *Bioorg Med Chem Lett* 2011;**21**:3095−8.
16. DeNinno MP, Wright SW, Etienne JB, Olson TV, Rocke BN, Corbett JW, et al. Discovery of triazolopyrimidine-based PDE8B inhibitors: exceptionally ligand-efficient and lipophilic ligand-efficient compounds for the treatment of diabetes. *Bioorg Med Chem Lett* 2012;**22**:5721−6.
17. Huang Y, Wu XN, Zhou Q, Wu Y, Zheng D, Li Z, et al. Rational design of 2-chloroadeninederivatives as highly selective phosphodiesterase 8A inhibitors. *J Med Chem* 2020;**63**:15852−63.
18. Card GL, England BP, Suzuki Y, Fong D, Powell B, Lee B, et al. Structural basis for the activity of drugs that inhibit phosphodiesterases. *Structure* 2004;**12**:2233−47.
19. Zhu J, Yang Q, Dai D, Huang Q. X-ray crystal structure of phosphodiesterase 2 in complex with a highly selective, nanomolar inhibitor reveals a binding-induced pocket important for selectivity. *J Am Chem Soc* 2013;**135**:11708−11.
20. Baell JB, Holloway GA. New substructure filters for removal of pan assay interference compounds (PAINS) from screening libraries and for their exclusion in bioassays. *J Med Chem* 2010;**53**:2719−40.
21. Yoshizaki K, Adachi K, Kataoka S, Watanabe A, Tabira T, Takahashi K, et al. Chronic cerebral hypoperfusion induced by right unilateral common carotid artery occlusion causes delayed white matter lesions and cognitive impairment in adult mice. *Exp Neurol* 2008;**210**:585−91.
22. Zhao Y, Gu JH, Dai CL, Liu Q, Iqbal K, Liu F, et al. Chronic cerebral hypoperfusion causes decrease of *O*-GlcNAcylation, hyperphosphorylation of tau and behavioral deficits in mice. *Front Aging Neurosci* 2014;**6**:10.
23. Wohl A. Bromierung ungesättigter Verbindungen mit N-Brom-acetamid, ein Beitrag zur Lehre vom Verlauf chemischer Vorgänge. *Ber Dtsch Chem Ges* 1919;**52**:51−63.
24. Ziegler K, Schenck G, Krockow EW, Siebert A, Wenz A, Weber H. Die synthese des cantharidins. *Justus Liebigs Ann Chem* 1942;**551**: 1−79.
25. Miyaura N, Suzuki A. Palladium-catalyzed cross-coupling reactions of organoboron compounds. *Chem Rev* 1995;**95**:2457−83.
26. Li Z, Lu X, Feng LJ, Gu Y, Li X, Wu Y, et al. Molecular dynamics-based discovery of novel phosphodiesterase-9A inhibitors with non-pyrazolopyrimidinone scaffolds. *Mol Biosyst* 2015;**11**:115−25.
27. Wu XN, Huang YD, Li JX, Yu YF, Zhou Q, Zhang C, et al. Structure-based design, synthesis, and biological evaluation of novel pyrimidinone derivatives as PDE9 inhibitors. *Acta Pharm Sin B* 2018;**8**:615−28.
28. Miyamoto S, Kollman PA. SETTLE: an analytical version of the SHAKE and RATTLE algorithm for rigid water models. *J Comput Chem* 1992;**13**:952−62.
29. Ryckaert JP, Ciccotti G, Berendsen HJ. Numerical integration of the Cartesian equations of motion of a system with constraints: molecular dynamics of *N*-alkanes. *J Comput Phys* 1977;**23**:327−41.
30. Essmann U, Perera L, Berkowitz ML, Darden T, Lee H, Pedersen LG. A smooth particle mesh Ewald method. *J Chem Phys* 1995;**103**: 8577−93.
31. Darden T, York D, Pedersen L. Particle mesh Ewald: an N.log(N) method for Ewald sums in large systems. *J Chem Phys* 1993;**98**: 10089−92.
32. Hou TJ, Wang JM, Li YY, Wang W. Assessing the performance of the MM/PBSA and MM/GBSA Methods. 1. The accuracy of binding free energy calculations based on molecular dynamics simulations. *J Chem Inf Model* 2011;**51**:69−82.
33. Xu L, Sun H, Li Y, Wang J, Hou T. Assessing the performance of MM/PBSA and MM/GBSA Methods. 3. The impact of force fields and ligand charge models. *J Phys Chem B* 2013;**117**:8408−21.
34. Massova I, Kollman PA. Combined molecular mechanical and continuum solvent approach (MM-PBSA/GBSA) to predict ligand binding. *Perspect Drug Discov* 2000;**18**:113−35.
35. Case DA, Aktulga HM, Belfon K, Ben-Shalom IY, Brozell SR, Cerutti DS, et al. *Amber 2021*. San Francisco: University of California; 2021.
36. Wang H, Yan Z, Yang S, Cai J, Robinson H, Ke H. Kinetic and structural studies of phosphodiesterase-8A and implication on the inhibitor selectivity. *Biochemistry* 2008;**47**:12760−8.
37. Yan Z, Wang H, Cai J, Ke H. Refolding and kinetic characterization of the phosphodiesterase-8A catalytic domain. *Protein Expr Purif* 2009; **64**:82−8.
38. Wu Y, Tian YJ, Le ML, Zhang SR, Zhang C, Huang MX, et al. Discovery of novel selective and orally bioavailable phosphodiesterase-1 inhibitors for the efficient treatment of idiopathic pulmonary fibrosis. *J Med Chem* 2020;**63**:7867−79.
39. Wu D, Huang Y, Chen Y, Huang YY, Geng H, Zhang T, et al. Optimization of chromeno[2,3-*c*]pyrrol-9(2*H*)-ones as highly potent, selective, and orally bioavailable PDE5 inhibitors: structure−activity relationship, X-ray crystal structure, and pharmacodynamic effect on pulmonary arterial hypertension. *J Med Chem* 2018;**61**:8468−73.
40. Yang Y, Zhang S, Zhou Q, Zhang C, Gao Y, Wang H, et al. Discovery of highly selective and orally available benzimidazole-based phosphodiesterase 10 inhibitors with improved solubility and pharmacokinetic properties for treatment of pulmonary arterial hypertension. *Acta Pharm Sin B* 2020;**10**:2339−47.
41. Wang H, Liu Y, Chen Y, Robinson H, Ke H. Multiple elements jointly determine inhibitor selectivity of cyclic nucleotide phosphodiesterases 4 and 7. *J Biol Chem* 2005;**280**:30949−55.